JOURNAL OF GEOPHYSICAL RESEARCH, VOL. 97, NO. D4, PAGES 3711–3724, MARCH 20, 1992

Intercomparison and Interpretation of Surface Energy Fluxes in Atmospheric General Circulation Models

D. A. RANDALL,[1] R. D. CESS,[2] J. P. BLANCHET,[3] G. J. BOER,[3] D. A. DAZLICH,[1] A. D. DEL GENIO,[4] M. DEQUE,[5] V. DYMNIKOV,[6] V. GALIN,[6] S. J. GHAN,[7] A. A. LACIS,[4] H. LE TREUT,[8] Z.-X. LI,[8] X.-Z. LIANG,[9] B. J. MCAVANEY,[10] V. P. MELESHKO,[11] J. F. B. MITCHELL,[12] J.-J. MORCRETTE,[13] G. L. POTTER,[7] L. RIKUS,[10] E. ROECKNER,[14] J. F. ROYER,[5] U. SCHLESE,[14] D. A. SHEININ,[11] J. SLINGO,[15] A. P. SOKOLOV,[11] K. E. TAYLOR,[7] W. M. WASHINGTON,[16] R. T. WETHERALD,[17] I. YAGAI,[18] AND M.-H. ZHANG[2]

We have analyzed responses of the surface energy budgets and hydrologic cycles of 19 atmospheric general circulation models to an imposed, globally uniform sea surface temperature perturbation of 4 K. The responses of the simulated surface energy budgets are extremely diverse and are closely linked to the responses of the simulated hydrologic cycles. The response of the net surface energy flux is not controlled by cloud effects; instead, it is determined primarily by the response of the latent heat flux. The prescribed warming of the oceans leads to major increases in the atmospheric water vapor content and the rates of evaporation and precipitation. The increased water vapor amount drastically increases the downwelling infrared radiation at the Earth's surface, but the amount of the change varies dramatically from one model to another.

1. INTRODUCTION

Cess et al. [1989, 1990] presented results from a large fraction of the world's atmospheric general circulation models (GCMs) illustrating their responses to prescribed changes in the sea surface temperature (SST) distribution. Two runs were made with each model: one with the SSTs reduced by an arbitrary and geographically uniform 2 K from the observed climatological July SSTs and a second with the SSTs arbitrarily increased by 2 K from their climatological values. Other input data used in both of the runs conformed with observed July conditions.

The results were analyzed to determine the "global sensitivity" of the various models, defined as the ratio of the change of the globally averaged surface air temperature to the change of the globally averaged net radiation at the top of the atmosphere. The global sensitivities ranged over a factor of 3. Further analysis revealed that virtually all of this variation among the models could be accounted for by differences in the simulated cloud feedbacks of the various models.

Despite the compelling and satisfying simplicity of this conclusion, there are unanswered questions and many aspects of the intercomparison results that require further study. Since identical SST perturbations were used in all of the models, the simulated response of the surface air temperature was nearly the same in all cases. Intermodel differences in global sensitivity were therefore mainly revealed by differences in the response of the net radiation at the top of the atmosphere. Since the atmospheric energy budgets of the models are nearly in balance (the averaging periods used were 30 days or more, depending on the model), there were corresponding differences in the simulated changes of the net surface energy fluxes. (This is illustrated later.) In fact, since the perturbation was imposed at the sea surface, the most direct response of the models was to alter their surface energy fluxes.

The surface energy fluxes include the turbulent fluxes of sensible and latent heat, as well as terrestrial and solar radiative energy fluxes. The radiation fluxes can be broken down further, e.g., into clear sky and cloudy components or into upward and downward components. In a time average over tens of days or longer the globally averaged surface latent heat flux is obviously proportional to the globally averaged precipitation (they are equal, apart from a unit's conversion). The surface energy budget and the hydrologic cycle are thus closely related.

[1]Department of Atmospheric Science, Colorado State University, Fort Collins.
[2]Institute for Terrestrial and Planetary Atmospheres, State University of New York, Stony Brook.
[3]Atmospheric Environment Service, Canadian Climate Center, Downsview, Ontario.
[4]Goddard Institute for Space Studies, National Aeronautics and Space Administration, New York.
[5]Direction de la Meteorologie, Centre National de Recherches Meteorologiques, Toulouse, France.
[6]Department of Numerical Mathematics, Academy of Sciences, Moscow, Russia.
[7]Program for Climate Model Diagnosis and Intercomparison, Lawrence Livermore National Laboratory, Livermore, California.
[8]Laboratoire de Meteorologie Dynamique, Paris, France.
[9]Department of Mechanical Engineering, State University of New York, Stony Brook.
[10]Bureau of Meteorology Research Centre, Melbourne, Victoria, Australia.
[11]Voeikov Main Geophysical Observatory, St. Petersburg, Russia.
[12]Meteorological Office, Bracknell, Berkshire, England.
[13]European Centre for Medium-Range Weather Forecasts, Reading, Berkshire, England.
[14]Meteorologisches Institut, University of Hamburg, Germany.
[15]Department of Meteorology, University of Reading, Berkshire, England.
[16]Climate and Global Dynamics Division, National Center for Atmospheric Research, Boulder, Colorado.
[17]National Oceanic and Atmospheric Administration/Geophysical Fluid Dynamics Laboratory, Princeton University, Princeton, New Jersey.
[18]Meteorological Research Institute, Ibakari-Ken, Japan.

Paper number 91JD03120.
0148-0227/92/91JD-03120$05.00

This paper reports the results of a further analysis of the same model simulations discussed by *Cess et al.* [1990, hereafter referred to as C90]. In the present study we focus on the response of the surface energy budget and the hydrologic cycle to the imposed SST changes. A motivation for our study is the critical role of the surface energy budget in climate change, as discussed by *Ramanathan* [1981]. He investigated the changes in the surface energy budget induced by a CO_2 doubling, as simulated by a simple one-dimensional climate model. He found that the direct warming by CO_2 is actually a minor component in the changes of the surface energy balance. As the surface warms, evaporation increases, leading to a major increase in the atmospheric water vapor content. Mainly because of the increased absolute humidity, the atmosphere radiates down more strongly on the surface, heating it. In fact, even though the surface temperature increases, the net longwave cooling of the surface actually decreases. The changes in the surface energy budget are thus dominated by the increased cooling by the latent heat flux and the decreased infrared cooling. In accordance with *Ramanathan*'s [1981] analysis, the changes in the surface sensible heat flux and solar radiation play relatively minor roles. In short, *Ramanathan* [1981] showed that the sensitivity of the climate to external perturbations such as increasing CO_2 concentrations is strongly influenced by the responses of the surface energy budget and the hydrologic cycle to an increase in the SST. (More recently, however, *Ramanathan and Collins* [1991] have argued that changes in solar radiation (due to changes in cloudiness) provide a major negative feedback that resists warming of the tropical oceans.)

The model results produced for the GCM Intercomparison provide us with an unprecedented opportunity to investigate the degree to which existing GCMs agree on the response of the surface energy budget to an increase in the SST. This paper reports the results of such an investigation.

Gutowski et al. [1991] recently investigated the surface energy budgets simulated by the Geophysical Fluid Dynamics Laboratory (GFDL), Goddard Institute for Space Studies (GISS), and National Center for Atmospheric Research (NCAR) GCMs in multiyear simulations of both the present climate and a doubled CO_2 climate. All three of these models included slab oceans with prognostic sea surface temperatures. Gutowski et al. showed how the surface energy budgets of the three GCMs responded to increased CO_2 levels both globally and regionally and for the various seasons of the year.

Although the present study has much in common with that of *Gutowski et al.* [1991], it differs in several important ways. First, we have drastically simplified the physical issues by prescribing identical sea surface temperature perturbations for all models; the results analyzed by Gutowski et al. involved computed SST perturbations that differed from model to model, both globally and geographically. Second, as already mentioned, we have employed perpetual July conditions. Third, we have pooled results from 19 GCMs, whereas *Gutowski et al.* [1991] analyzed results from only three models. In view of these differences, Gutowski's study and ours are complementary.

In this paper we attempt to relate differences in results to differences in formulation. This is not an easy task because with only a few exceptions, pairs of participating models differ not just in one way but in many ways. Some tentative conclusions can be drawn, however, and suggest promising avenues for further exploration by individual investigators.

2. What Was Computed and How

It is important to keep in mind that although the runs discussed here involve surface warming, they are not simulations of the response of the climate system to increasing CO_2 concentrations and are not even particularly good analogs to such runs. First of all, these are "perpetual July" simulations, rather than the seasonally varying runs that would be required for realistic climate change simulations. Second, we have increased and/or decreased the SSTs in a deliberately idealized, patently unrealistic fashion. Although simulations of the climatic response to a CO_2 doubling sometimes produce a globally averaged surface warming of about 4 K, they never produce a 4 K warming of the tropical oceans, such as that imposed here [*Houghton et al.*, 1990]. Finally and importantly, although the globally and annually averaged net surface energy flux must be close to zero in a $2 \times CO_2$ simulation that is close to equilibrium, no such constraint applies in the present runs because the SSTs are fixed so that the oceans represent an infinite energy reservoir.

Table 1 lists the 19 GCMs whose results are analyzed in this paper. For the most part, these are the same models that participated in the study of C90. Exceptions are the European Center for Medium-Range Weather Forecasting (ECMWF) model, a newer version of which has been used in the present study, and the 17-level version of the Colorado State University (CSU) model, which supplements the 9-level version used by C90. Except in a few cases the model runs used in the present study are identical to those discussed by C90.

References describing the formulations of the various models were given by C90, who also defined the various acronyms that are used to name the models. Table 1 gives further relevant information on each model's formulation and records which method was used to determine "clear sky" fluxes (discussed below) and whether or not the ground wetness was fixed. This last point is pertinent because the northern hemisphere continents tend to dry out unrealistically in perpetual July simulations, unless of course the ground wetness is artificially fixed.

Inspection of Table 1 shows that grid point and spectral models are about equally represented; a majority of the models include the effects of the water vapor continuum in their longwave radiation parameterization, although the details differ from model to model; about half the models use a convective parameterization based on the mass flux approach; almost all of the models incorporate Monin-Obukhov similarity theory in their boundary layer parameterizations; only about half the models include the diurnal cycle of insolation; a majority of the models do not include an explicit parameterization of shallow cumulus convection; the surface cloud radiative forcing was not available from four of the models, and of the remaining 15, 11 determined the surface cloud radiative forcing by method 2 (discussed below); and finally that most of the models allowed the ground wetness to evolve in response to the simulated perpetual July patterns of precipitation and evaporation, thus tending to cause the northern hemisphere continents to dry out and warm up.

TABLE 1. Summaries of Some Relevant Aspects of Each Model's Design

Model	Convective Parameterization	Water Vapor Continuum	Boundary Layer Parameterization	Shallow Convection	Diurnal Cycle	CF Method (Surface)	Ground Wetness	Horizontal Discretization
CCC	MCA	Yes	MO with K theory	No	Yes	2	Computed	Spectral
CSU 9L	Mass flux (Arakawa-Schubert)	Yes	Variable depth mixed layer, MO	Yes, based on CTEI	Yes	2	Fixed	Grid point
CSU 17L	Mass flux (Arakawa-Schubert)	Yes	Variable depth mixed layer, MO	Yes, based on CTEI	Yes	2	Fixed	Grid point
GFDL I	MCA	Yes	MO with K theory	No	No	1	Computed	Spectral
GFDL II	MCA	Yes	MO with K theory	No	No	1	Computed	Spectral
ECHAM Diag.	Kuo	Yes	MO with K theory	Yes	No	2	Computed	Spectral
ECHAM Prog.	Kuo	Yes	MO with K theory	Yes	No	2	Computed	Spectral
CCM/LLNL	MCA	No	MO with K theory	No	No	2	Fixed	Spectral
MRI	Mass flux (Arakawa-Schubert)	No	Variable depth mixed layer, MO	No	Yes	not available	Computed	Grid point
NCAR CCM0	MCA	No	Bulk aerodynamic with K theory	No	No	not available	Computed	Spectral
UKMO	Mass flux	Yes	MO with K theory	No	Yes	2	Fixed	Grid point
DMN/CNRM	Mass flux (Bougeault)	Yes	MO with K theory	Yes	Yes	1	Computed	Spectral
OSU/IAP	Mass flux (Early Arakawa)	No	MO with K theory	No	Yes	1	Computed	Grid point
BMRC	Kuo	Yes	MO with K theory	Yes	No	not available	Computed	Spectral
LMD	Kuo with MCA	Yes	MO with K theory	No	No	2	Computed	Grid point
ECMWF	Mass flux (Tiedtke)	Yes	MO with K theory	Yes	Yes	2	Computed	Spectral
GISS	Mass flux [*Hansen et al.* [1983]	Yes	MO with K theory	No	Yes	not available	Computed	Grid point
DNM	MCA	No	MO with K theory	No	No	2	Computed	Grid point
MGO	Kuo	Yes	MO with K theory	Yes	No	2	Computed	Spectral

MCA refers to moist convective adjustment. MO refers to Monin-Obukhov similarity. CTEI refers to cloud top entrainment instability. CF method (surface) refers to the method used to determine the clear sky surface radiation. Models ae identified in text.

The following notation will be useful:

N net surface energy flux;
LW net terrestrial radiation at the surface (subscript "sfc") or at the top of the atmosphere (subscript "top");
SW net solar radiation at the surface (subscript sfc) or at the top of the atmosphere (subscript top);
R net radiation at the surface (subscript sfc) or at the top of the atmosphere (subscript top);
LWCF longwave cloud radiative forcing at the surface (subscript sfc) or at the top of the atmosphere (subscript top);
SWCF solar cloud radiative forcing at the surface (subscript sfc) or at the top of the atmosphere (subscript top);
RCF total cloud radiative forcing at the surface (subscript sfc) or at the top of the atmosphere (subscript top);
$LW\uparrow$ upward longwave flux at the surface;
$LW\downarrow$ downward longwave flux at the surface;
$SW\uparrow$ upward shortwave flux at the surface;
$SW\downarrow$ downward shortwave flux at the surface;
H surface sensible heat flux;
LH surface latent heat flux;
P precipitation rate;
PW precipitable water content (vertically integrated water vapor amount).

For all energy fluxes, our sign convention is that positive values denote an energy flux into the surface (or into the top of the atmosphere).

An important relationship among the fluxes is

$$N = SW + LW + SH + LH. \quad (1)$$

Of course, SW and LW can be further broken down into their upward and downward components or into their clear sky and cloud-forcing components.

The subscript "clr" will be used to denote clear sky values, as determined by methods 1 or 2 of *Cess and Potter* [1987]. Briefly, method 1 defines clear sky fluxes only for those grid columns that are actually cloud free, while method 2 defines clear sky fluxes for all columns, regardless of whether or not clouds are actually predicted by the model. Table 1 indicates which method was used by each modeling group. As discussed by *Harshvardhan et al.* (1989), there are significant differences in the results obtained with the two methods, for models that include the diurnal cycle. These differences are particularly noticeable in the clear sky solar

TABLE 2. The Components of the Globally Averaged Surface Energy Budget in the −2 K Runs,

−2 K RUNS	CCC	CSU 9L	CSU 17L	GFDL I	GFDL II	ECHAM Diag.	ECHAM Prog.	CCM/ LLNL	MRI	NCAR CCM0
N	3.22	−1.52	−9.17	−4.99	−6.80	−18.12	−5.82	−38.03	11.80	−5.91
SW	170.64	173.73	166.71	157.80	176.83	133.94	139.95	146.27	181.64	166.90
LW	−66.26	−68.19	−62.44	−69.51	−69.37	−71.42	−69.06	−65.58	−72.86	−55.60
R	104.38	105.54	104.27	88.29	107.46	62.52	70.89	80.69	108.78	111.3
LH	−74.55	−104.13	−107.64	−68.74	−81.46	−64.32	−60.64	−94.02	−82.62	−101.47
SH	−26.66	−2.94	−5.80	−25.54	−32.80	−16.32	−16.08	−24.70	−14.36	−9.83
$LW\downarrow$	330.03	320.66	325.52	334.10	334.07			324.99		
$SW\downarrow$	195.70	198.39	190.80	180.13	202.34			169.14		
$LW\uparrow$	−396.29	−388.85	−387.96	−403.61	−403.44			−390.57		
$SW\uparrow$	−25.06	−24.66	−24.09	−22.33	−25.51			−22.87		
SW_{clr}	244.62	228.53	228.38	222.37	222.91	191.39	195.51	221.14		
LW_{clr}	−94.39	−96.19	−94.03	−102.24	−104.42	−94.29	−96.84	−97.70		
R_{clr}	150.23	132.34	134.35	120.13	118.49	97.1	98.67	123.44		
SWCF	−73.98	−54.80	−61.67	−64.62	−46.08	−57.45	−55.56	−74.87		
LWCF	28.13	28.00	31.59	32.76	35.05	22.87	27.78	32.12		
RCF	−45.85	−26.80	−30.09	−31.85	−11.03	−34.58	−27.78	−42.75		

All units are W m^{-2}.

radiation. The intercomparison participants have concluded that method 2 allows the simplest, most straightforward intercomparison of models, even though method 1 is advantageous for comparing a model with observations. Whenever possible, we have used the method 2 results in this paper. Unfortunately, however, method 2 diagnostics are not available from all of the models (see Table 1), so the results presented below are based on a perplexing mixture of methods 1 and 2 diagnostics. The same is true of the results discussed by C90. For nondiurnal models (e.g., the two GFDL models), the difference between methods 1 and 2 may be unimportant. The only diurnal models that did not report method 2 results are DMN/CNRM and OSU/IAP.

For convenience, a result obtained in a "−2 K" run will be denoted by (−2). For example, the precipitation obtained in a −2 K run will be denoted by $P(-2)$. The notation $\Delta(\ )$ will indicate a response to the prescribed SST increase. For example, $\Delta(PW)$ will denote the PW obtained in the +2 K run, minus the PW obtained in the −2 K run.

All of the variables listed above were saved by some of the models; some of the variables were saved by only a subset of the models. Some of the models saved zonal means, while others saved only global means.

3. Surface Energy Fluxes in the −2 K Climate

Table 2 summarizes the components of the globally averaged surface energy budget in the −2 K runs, as simulated by the various GCMs. The last two columns of the table show the means and standard deviations for each quantity, after the largest and smallest values have been discarded.

The globally averaged net surface energy fluxes simulated by the various models range from −38 to about 15 W m^{-2}, a startling span of more than 50 W m^{-2}. Positive values of N might be expected in the −2 K simulations, since this would tend to increase the SSTs (if we let them change), thus driving the system toward the observed climate. The largest positive N occurs in the ECMWF model. Models which produce negative values of $N(-2)$ apparently "want to" further cool the oceans, even though the SSTs are already prescribed to be 2 K colder than observed. The largest negative N occurs in the CCM/LLNL model, which has an anomalously high planetary albedo due to excessively bright clouds. The same model also has particularly strong surface fluxes of both sensible and latent heat. We caution that it is not possible to draw firm conclusions as to climatic equilibrium on the basis of these perpetual July simulations. Annual cycle simulations would be required to determine whether or not the various models are in climatic equilibrium with the reduced SSTs.

The models disagree to a surprising degree over such a seemingly simple statistic as the globally averaged clear sky surface solar radiation. The values range from 191 to 244 W m^{-2}, spanning about 50 W m^{-2}. The ECHAM and DNM models have particularly low values of $(SW)_{clr}$. The wide range of $(SW)_{clr}$, among the models, may be accounted for by the following:

(1) Differences in the prescribed "solar constant." It would be useful to adopt a standard value of the solar constant for use in future GCM intercomparisons.

(2) Differences in diurnally averaged clear sky atmospheric absorption [*Fouquart et al.*, 1991], which are caused by differences in the solar radiation parameterizations. Such differences might arise, in particular, between models that include the diurnal cycle and those that do not. The results presented in Table 2 suggest that models with the diurnal cycle tend to absorb more clear sky solar radiation than those without.

(3) Differences in diurnally averaged clear sky atmospheric absorption which are caused by differences in absorber amounts (e.g., water vapor).

(4) Surface albedo differences among the models. We have investigated the extent to which intermodel differences in the surface albedo (defined as $SW\uparrow/SW\downarrow$) can account for differences in $(SW)_{clr}$, for those models that reported $SW\uparrow$ and $SW\downarrow$. No strong relationship exists, and we conclude that differences in surface albedo are not the dominant factor. Note, however, that the information available to us here allows determination of only the all-sky surface albedo; we cannot evaluate the clear sky surface albedo.

(5) Cloud effects. The surface albedo for diffuse radiation is normally higher, in an overall energy-weighted sense, than

As Simulated by the Various GCMs

UKMO	DMN/ CNRM	OSU/ IAP	BMRC	LMD	ECMWF	GISS	DNM	MGO	Mean	SD
−6.52	−2.20	−18.81	3.66	0.49	15.00	−4.46	−11.72	−1.93	−4.64	7.56
160.55	164.46	146.65	170.87	155.48	168.21	168.20	156.86	165.52	162.10	10.34
−56.07	−73.22	−64.54	−62.58	−58.43	−69.07	−52.7	−85.00	−63.35	−65.74	5.43
104.48	91.24	82.11	108.29	97.05	99.14	115.50	71.86	102.17	96.35	13.11
−90.07	−80.49	−74.27	−92.69	−84.25	−55.28	−82.70	−62.44	−77.29	−80.95	12.86
−20.93	−12.96	−26.62	−21.99	−12.31	−28.86	−36.40	−21.14	−26.81	−20.22	7.54
338.21	321.83		341.46		327.92	343.30	323.08		330.31	7.00
177.90	180.19		193.85		190.91	190.80	185.32		188.40	7.12
−394.28	−395.05		−404.04		−396.99	−396.00	−408.08		−396.91	5.32
−17.35	−15.73		−22.98		−22.70	−22.60	−28.45		−23.02	2.29
230.15	221.42	218.59		225.37	222.63		194.38	216.46	219.06	11.40
−81.77	−101.9	−106.19		−90.37	−100.27		−120.80	−97.02	−95.83	10.44
148.38	119.52	112.40		135.00	122.36		73.58	119.44	121.66	14.17
−69.60	−56.96	−71.94		−69.89	−54.42		−37.52	−50.94	−60.61	8.74
25.70	28.68	41.65		31.94	31.20		35.80	33.67	30.96	3.07
−43.90	−28.28	−30.29		−37.95	−23.22		−1.72	−17.27	−29.68	9.26

that for direct beam radiation. In the absence of clouds, direct beam radiation dominates, but clouds increase the relative contribution from diffuse radiation. Differences among the models in the simulated geographical distribution of cloudiness are sufficient, therefore, to produce differences in the simulated surface albedo. As mentioned above, the surface albedo values are based on the all-sky radiation and thus may differ from and are probably overestimates of the appropriate clear sky albedos for each model. Unfortunately, we lack sufficient information to determine the clear sky surface albedos for the various models.

The simulations of $LW_{clr}(-2)$ vary over about 40 W m^{-2}, from −82 to 120 W m^{-2}. This can be explained in terms of the differences in $PW(-2)$ (discussed later) and the fact that some models include the effects of the water vapor continuum, while others do not [*Ellingson et al.*, 1991; compare Table 1]. Differences in the method of computation of the near-surface air temperature may also play a role here.

In the model results, clouds tend to cool the Earth's surface through solar cloud forcing and to warm it through longwave cloud forcing. Table 2 shows that the cooling effect dominates at the surface, just as it does at the top of the atmosphere in both model results and observations [e.g., *Cess and Potter*, 1987; *Ramanathan et al.*, 1989]. The standard deviation of RCF_{top} is more than 9 W m^{-2}, even though the largest (DNM) and smallest (CCC) values have been discarded.

4. Global Mean Responses to a 4 K Warming of the Oceans

The main result of C90 is reproduced, in Figure 1, for the present ensemble of models. As indicated in the figure, the models disagree significantly on the "climate sensitivity parameter," $\Delta(T_S)/\Delta(R_{top})$, but these differences are very well explained by differences in $\Delta(RCF_{top})/\Delta(R_{top})$. In other words, differences in climate sensitivity are due mainly to differences in cloud feedback, at least for the case in which the sea ice distributions are fixed. Table 3 summarizes the simulated responses of the surface temperature and the top-of-the-atmosphere all-sky and clear sky radiation to the imposed SST increase.

Table 4 shows how the components of the surface energy budget change when the SST is increased from −2 K to +2 K. The response of the net surface energy flux, $\Delta(N)$, is of particular interest. The role of $\Delta(N)$ in the surface energy budget is closely analogous to that of $\Delta(R_{top})$. Intuition suggests that just as an increase in the SST led to negative values of $\Delta(R_{top})$ (cooling the planet), it should also lead to negative values of $\Delta(N)$ (cooling the Earth's surface). This is, in fact, the case for every model. The values of $\Delta(N)$ range, however, from about −2 to −11 W m^{-2}.

Note that the range of $\Delta(N)$ (9 W m^{-2}) is considerably less than that of $N(-2)$ (53 W m^{-2}). This raises an important point. It is sometimes suggested that in order for models to quantitatively simulate the response of the climate to a 4 W m^{-2} radiative forcing, such as that due to increased CO_2, it is necessary for the models to simulate the energy fluxes associated with the present climate state to an accuracy of 4 W m^{-2} or better. This mistaken idea is grounded in confusion between the value of a function and the value of its derivative. In the present context, the function in question is

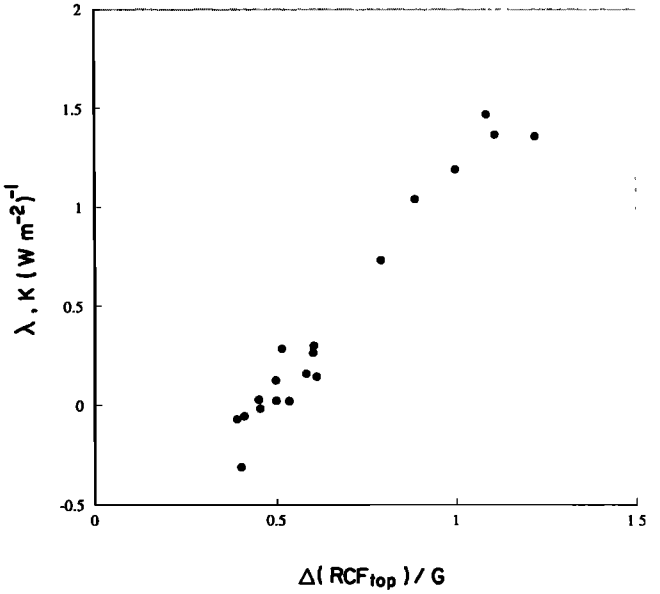

Fig. 1. The relationship between $\Delta(T_S)/\Delta(R_{top})$ and $\Delta(RCF_{top})/G$. Here G is the "forcing" defined by *Cess et al.* [1990]; it is equal to $-\Delta(R_{top})$.

TABLE 3. Responses of the Globally Averaged Surface Air Temperature (K) and the

+2 K MINUS −2 K	CCC	CSU 9L	CSU 17L	GFDL I	GFDL II	ECHAM Diag.	ECHAM Prog.	CCM/ LLNL	MRI	NCAR CCM0
$\Delta(T_S)$	4.38	4.16	4.08	3.97	4.15	3.93	3.92	3.84	4.36	4.02
$\Delta(LW_{top})$	−10.78	−11.66	−10.95	−8.33	−9.45	−11.01	−9.20	−8.90	−9.55	−12.06
$\Delta(SW_{top})$	−0.43	3.32	1.02	1.74	0.31	7.47	5.29	4.05	2.33	8.36
$\Delta(LW_{clr,\ top})$	−10.95	−9.11	−9.91	−8.61	−9.23	−10.23	−9.93	−9.17	−10.23	−9.69
$\Delta(SW_{clr,\ top})$	0.52	0.58	0.52	0.28	0.24	1.86	1.34	0.78	0.84	0.56
$\Delta(R_{top})$	−11.21	−8.34	−9.93	−6.59	−9.14	−3.55	−3.90	−4.85	−7.22	−3.70
$\Delta(R_{clr,\ top})$	−10.43	−8.53	−9.39	−8.33	−8.99	−8.37	−8.59	−8.49	−9.39	−9.13
$\Delta(SWCF_{top})$	−0.95	2.74	0.50	1.46	0.07	5.60	3.95	3.28	1.49	7.80
$\Delta(LWCF_{top})$	0.17	−2.55	−1.04	0.28	−0.22	−0.78	0.73	0.27	0.68	−2.37
$\Delta(RCF_{top})$	−0.78	0.19	−0.54	1.74	−0.15	4.82	4.68	3.54	2.17	5.43

$N(-2)$, and its derivative is $\Delta(N)$. Models that produce widely different values of $N(-2)$ may nevertheless agree fairly well on the value of $\Delta(N)$; examples can be found by inspection of Tables 2 and 4. Similarly, accurate simulation of the Earth's radiation budget for the present climate is not a necessary prerequisite for (or a guarantee of) an accurate simulation of the response to a radiative perturbation such as that due to increased CO_2. Similar comments were made by *Mitchell et al.* [1987].

Conservation of total energy requires that in a time average, $\Delta(R_{top})$ and $\Delta(N)$ should be equal for each model, apart from the work done by the atmosphere on the lower boundary. Figure 2 shows that this expectation is reasonably well borne out, although there is a lot of scatter. The scatter can arise in several ways. First, most GCMs conserve total energy only approximately. For example, only a few models take into account that kinetic energy dissipation represents a source of internal energy; most simply allow the dissipated kinetic energy to "disappear." This represents a spurious energy loss of a few W m^{-2}. A second contributing factor is that some of the model results are averaged over only 30 days, not long enough to make the energy storage term completely negligible. Finally, as already mentioned, the atmosphere does work on the oceans and on the land surface.

Figure 3 shows that intermodel differences in $\Delta(T_S)/\Delta(N)$ are fairly well correlated with differences in $\Delta(RCF_{top})/\Delta(N)$. This is not surprising in view of Figures 1 and 2. It means that differences in the top-of-the-atmosphere cloud forcing can account for most of the differences in the net surface energy flux.

It does not follow, however, that differences in the surface cloud forcing can account for differences in $\Delta(N)$. In fact, $\Delta(RCF_{top})$ and $\Delta(RCF_{sfc})$ are, in many cases, of opposite sign (see Tables 3 and 4). As shown in Table 4, 10 of the 15 models that reported the surface cloud radiative forcing (CRF) produced negative values of $\Delta(RCF_{sfc})$. Thus for many of the models, $\Delta(RCF_{top})$ tends to warm the planet while $\Delta(RCF_{sfc})$ tends to cool the surface.

Figure 4 demonstrates that in fact, no strong relationship exists between $\Delta(RCF_{sfc})$ and $\Delta(N)$. For most of the models, $\Delta(RCF_{sfc})$ is negative, as is $\Delta(N)$, but in almost every case, $\Delta(N)$ is larger, in an absolute sense, than $\Delta(RCF_{sfc})$. In other words, the change in the surface cloud forcing tends to cool the surface, but the total cooling of the surface is greater than that due to the change in cloud forcing alone. The CCC and ECMWF models give particularly large negative values of $\Delta(RCF_{sfc})$. If these two models are omitted, the remaining models fall along a fairly orderly curve.

A further complication is that $\Delta(RCF_{top})$ and $\Delta(RCF_{sfc})$ are markedly different because the atmosphere itself experiences a cloud forcing (the response of the atmospheric cloud forcing to the 4 K increase in SST is the difference between $\Delta(RCF_{sfc})$ and $\Delta(RCF_{top})$) and that the response of

TABLE 4. The Response of the Various Components of the Surface

+2 K MINUS −2 K	CCC	CSU 9L	CSU 17L	GFDL I	GFDL II	ECHAM Diag.	ECHAM Prog.	CCM/ LLNL	MRI	NCAR CCM0
N	−10.10	−8.42	−11.17	−7.11	−9.28	−3.78	−3.96	−4.72	−10.12	−1.83
SW	−5.02	0.01	−2.06	−1.30	−3.31	3.06	1.63	1.54	−0.03	4.27
LW	3.54	8.35	7.85	4.32	2.78	0.67	1.16	3.77	1.32	1.63
R	−1.48	8.36	5.79	3.02	−0.53	3.73	2.79	5.31	1.29	5.9
LH	−9.89	−19.98	−19.95	−12.60	−12.61	−8.99	−8.07	−12.36	−12.85	−7.76
SH	1.21	3.20	3.00	2.47	3.85	1.47	1.33	2.33	1.44	1.86
$LW\downarrow$	24.86	30.12	29.25	26.00	25.06			24.85		
$SW\downarrow$	−5.50	−0.18	−2.32	−1.51	−4.03			1.23		
$LW\uparrow$	−21.33	21.76	−21.40	−21.68	−22.28			−21.08		
$SW\uparrow$	0.49	0.19	0.26	0.21	0.72			0.31		
SW clear	−2.61	−3.53	−3.20	−3.39	−3.59	−2.31	−2.88	−2.96		
LW clear	7.85	12.88	12.27	6.34	4.75	4.03	5.05	9.45		
R clear	5.24	9.53	9.07	2.95	1.16	1.72	2.17	6.49		
SWCF	−2.41	3.54	1.14	2.15	0.28	5.37	4.51	4.50		
LWCF	−4.31	−4.53	−4.42	−2.00	−1.97	−3.36	−3.89	−5.68		
RCF	−6.73	−1.00	−3.28	0.14	−1.69	2.01	0.61	−1.18		

Top-of-the-Atmosphere Radiation (W m^{-2} to the Imposed 4 K SST Increase

UKMO	DMN/ CNRM	OSU/ IAP	BMRC	LMD	ECMWF	GISS	DNM	MGO	Mean	SD
3.85	4.04	4.13	4.30	4.08	3.74	4.03	3.74	3.82	4.02	0.17
−11.48	−10.34	−9.50	−13.46	−8.85	−6.19	−8.22	−10.92	−9.77	−10.14	1.37
4.87	2.22	1.49	5.42	4.25	−3.12	4.92	2.62	3.52	3.20	2.07
−8.09	−9.57	−11.03	−8.77	−9.97	−9.20	−7.78	−9.16	−7.40	−9.39	0.81
0.43	0.44	0.74	0.56	0.58	2.77	0.00	0.64	0.26	0.66	0.40
−6.61	−8.12	−8.01	−8.04	−4.60	−9.31	−3.30	−8.30	−6.25	−6.85	2.07
−7.66	−9.13	−10.29	−8.21	−9.39	−6.43	−7.78	−8.52	−7.14	−8.67	0.76
4.44	1.78	0.75	4.86	3.67	−5.89	5.11	1.98	3.26	2.59	1.91
−3.39	−0.77	1.53	−4.69	1.12	3.01	−0.48	−1.76	−2.33	−0.64	1.42
1.05	1.01	2.28	0.17	4.79	−2.88	4.63	0.22	0.93	1.81	1.99

the atmospheric cloud forcing differs greatly among the models. Of course, this is primarily a longwave effect. For all of the 15 models that reported the surface CRF, the response of the atmospheric CRF to the SST increase is a warming of a few W m^{-2}.

Figure 5 shows that the response of the shortwave cloud forcing at the top of the atmosphere is well correlated with that at the surface. The reason is simply that in all of the models the shortwave absorption by clouds (i.e., the atmospheric solar cloud forcing) is weak. Such strong correlations are not found, however, for the longwave cloud forcing or the net cloud forcing (not shown).

Table 5 gives the globally averaged $P(-2)$ and $PW(-2)$ as simulated by the various models. The simulated globally averaged values of P range from 2.08 to 3.69 mm d^{-1}, while the simulated globally averaged values of PW range from 17.10 to 27.09 mm. There is no systematic relationship among the models between $PW(-2)$ and $P(-2)$. For example, it is not true that the models with higher $PW(-2)$ tend to have higher (or, for that matter, lower) $P(-2)$. This lack of a systematic relationship between $P(-2)$ and $PW(-2)$ reflects the very wide range of precipitation parameterizations used in the models. Further discussion is given later.

Table 6 shows that when the SSTs are increased by 4 K (about 1.4%), the hydrologic cycles of the models respond in dramatic fashion. Both PW and P increase for all of the models. The values of $\Delta(P)$ range from 0.29 to 0.69 mm d^{-1} and those of $\Delta(PW)$ range from 4.88 to 10.756 mm, more than a factor of 2 for both variables. These increases are of the order of 10–30% of the corresponding values in the −2 K runs. *Mitchell et al.* [1987] and *Mitchell and Ingram* [1991] discuss the changes in PW per degree of warming in several experiments with the UKMO model.

Which component fluxes are dominating $\Delta(N)$? Recall that

$$\Delta(N) = \Delta(SW) + \Delta(LW) + \Delta(SH) + \Delta(LH). \quad (2)$$

The values of $\Delta(SW_{clr,sfc})$ produced by the various models are all fairly consistent, near −2 or −3 W m^{-2}. These reductions can be explained in terms of increased atmospheric solar absorption due to the positive values of $\Delta(PW)$. The responses in the globally averaged all-sky SW are fairly modest but much more variable among the models, ranging from −8.25 to 4.27 W m^{-2}. The differences in $\Delta(SW_{sfc})$ are, of course, mainly due to differences in $\Delta(SWCF_{sfc})$.

For each model, $\Delta(LW_{sfc})$ is positive, as anticipated by *Ramanathan* [1981]. Note, however, that $\Delta(LW_{sfc})$ ranges from 0.07 to 8.35 W m^{-2}. Since the SST increase is the same in all of the models, one would expect that the changes in the $LW\uparrow$ would be nearly the same as well; Table 4 confirms this for those models that reported $LW\uparrow$. The standard deviation of $\Delta(LW\uparrow)$ is less than 2% of the mean.

The differences in $\Delta(LW_{sfc})$ are therefore primarily due to differences in $LW\downarrow$. The latter are due to both $\Delta LWCF_{sfc}$ and $\Delta(LW_{clr,sfc})$. Inspection of Table 4 shows that in every

Energy Budget When the SST Is Increased by 4 K

UKMO	DMN/ CNRM	OSU/ IAP	BMRC	LMD	ECMWF	GISS	DNM	MGO	Mean	SD
−7.26	−9.64	−5.09	−10.94	−7.69	−9.31	−3.54	−10.83	−7.56	−7.61	2.55
1.70	−1.64	1.54	2.50	2.56	−8.25	4.00	−3.20	1.16	0.39	2.55
6.14	4.95	2.21	4.32	1.90	4.97	2.90	1.17	0.07	3.27	1.98
7.84	3.31	3.75	6.82	4.46	−3.28	6.90	−2.03	1.23	3.42	2.95
−16.21	−16.04	−11.46	−14.18	−12.42	−8.47	−12.00	−8.96	−9.45	−12.15	3.17
1.11	3.08	2.62	−0.07	0.27	2.44	1.40	0.16	0.66	1.77	0.96
27.87	27.84		26.09		24.50	25.20	23.15		26.15	1.62
2.28	−1.56		2.55		−9.21	4.10	−4.09		−1.31	2.78
−21.73	−22.89		−21.78		−19.53	−22.30	−21.98		−21.73	0.39
−0.58	−0.07		−0.05		0.96	−0.10	0.88		0.28	0.33
−2.90	−3.65	−2.93		−2.75	−2.69		−2.98	−2.38	−2.98	0.36
10.44	6.90	8.33		7.23	8.50		1.82	3.69	7.29	2.56
7.54	3.25	5.40		4.48	5.81		−1.16	1.31	4.35	2.51
4.60	2.01	4.47		5.31	−5.56		−0.22	3.54	2.58	2.33
−4.30	−1.95	−6.12		−5.39	−3.53		−0.65	−3.62	−3.80	1.28
0.30	0.06	−1.65		−0.08	−9.09		−0.87	−0.08	−1.19	1.98

All units are W m^{-2}.

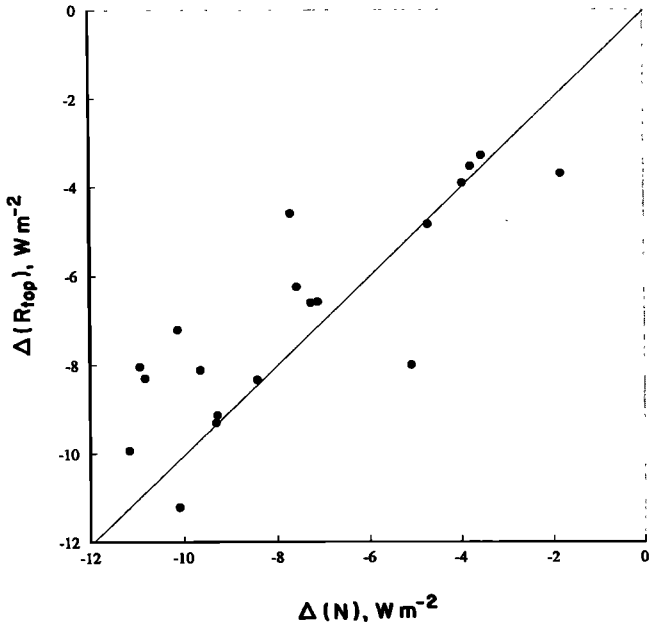

Fig. 2. The relationship between $\Delta(N)$ and $\Delta(R_{top})$. The thin diagonal line shows the curve along which these two quantities are equal. Approximate equality is to be expected. See text for details.

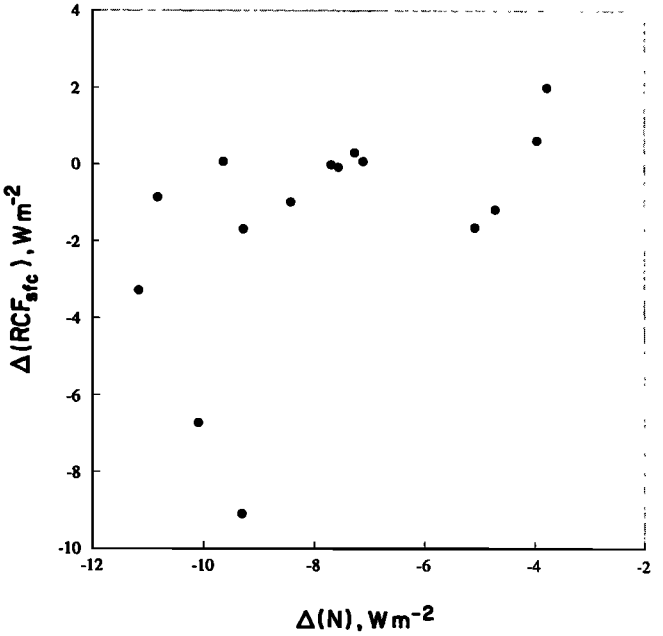

Fig. 4. The relationship between $\Delta(N)$ and $\Delta(\mathrm{RCF}_{sfc})$.

single case, $\Delta(LW_{sfc})$ and $\Delta(\mathrm{LWCF}_{sfc})$ have opposite signs; $\Delta(\mathrm{LWCF}_{sfc})$ is negative and $\Delta(LW_{sfc})$ is positive. This clearly shows that $\Delta(LW_{sfc})$ is being driven primarily by clear sky effects; $\Delta(\mathrm{LWCF}_{sfc})$ is of secondary importance. We then conclude that the simulated values of $\Delta(LW_{sfc})$ are essentially determined by the response of the clear sky downward component of the surface longwave radiation. In other words, when the SST increases, the clear sky downward longwave radiation at the surface increases; this can result from an increase in the atmospheric temperature and/or from an increase in the effective emissivity of the boundary layer. An increase in the clear sky emissivity tends to diminish the longwave cloud forcing; if the clear sky is already opaque, adding a cloud makes little difference. The fact that for all of the models $\Delta(\mathrm{LWCF}_{sfc})$ is negative while $\Delta(LW_{sfc})$ is positive strongly suggests that the negative values of $\Delta(\mathrm{LWCF}_{sfc})$ result from increases in the clear sky emissivity and therefore that the increases in the clear sky downward emission are, in part, due to increases in the emissivity of the boundary layer air.

Obviously, this suggests that differences in $\Delta(PW)$ are strongly influencing $\Delta(LW_{sfc})$. Figure 6 shows, however, that there is no strong relationship between $\Delta(LW_{clr,sfc})$ and $\Delta(PW)$. The lack of order in this figure may result from

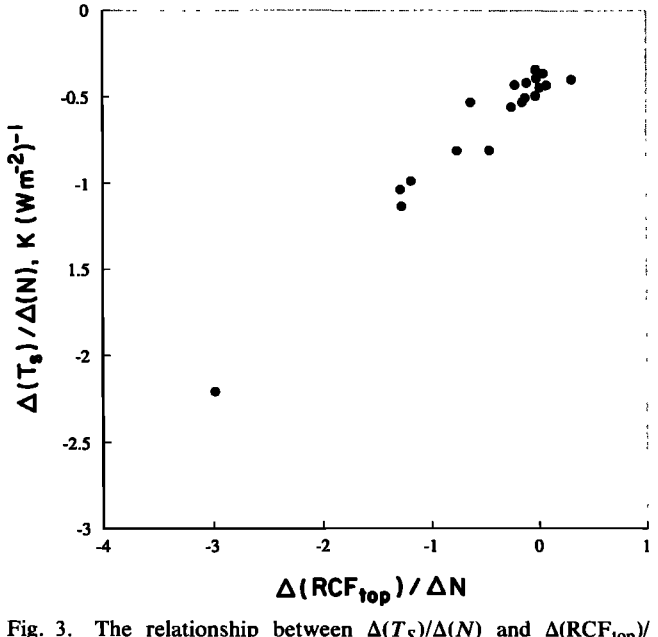

Fig. 3. The relationship between $\Delta(T_S)/\Delta(N)$ and $\Delta(\mathrm{RCF}_{top})/\Delta(N)$.

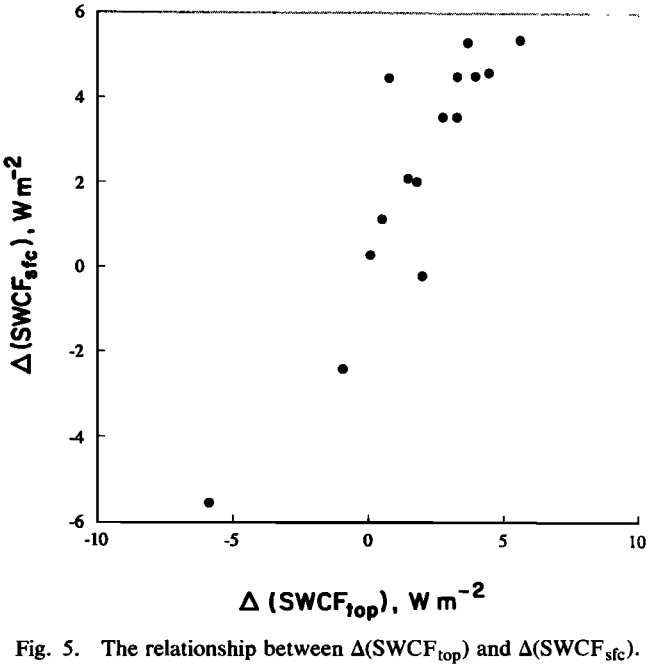

Fig. 5. The relationship between $\Delta(\mathrm{SWCF}_{top})$ and $\Delta(\mathrm{SWCF}_{sfc})$.

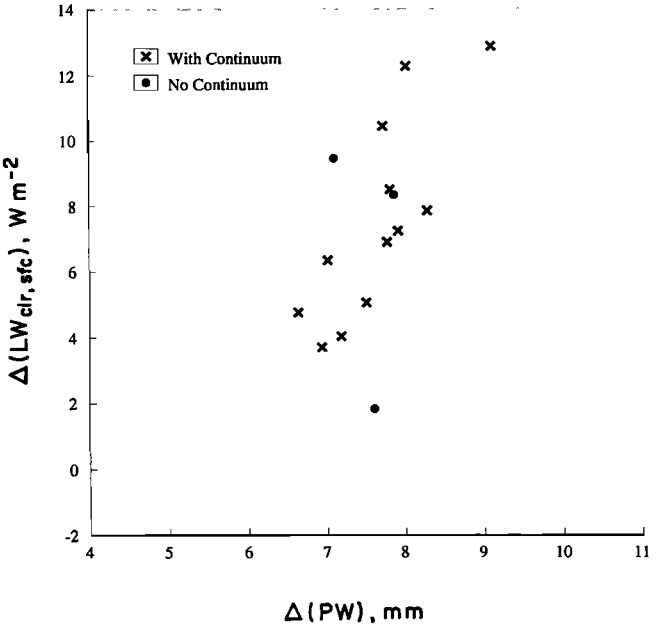

Fig. 6. The relationship between $\Delta(LW_{clr,sfc})$ and $\Delta(PW)$.

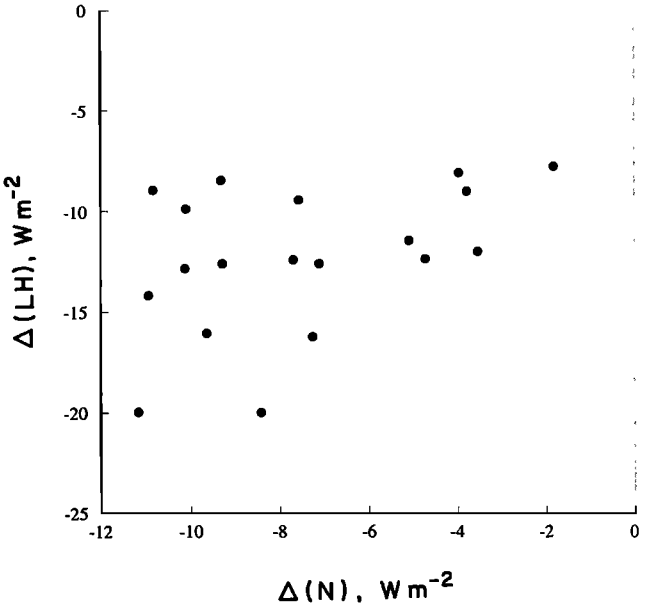

Fig. 8. The relationship between $\Delta(N)$ and $\Delta(LH)$.

differences in the radiation parameterizations used in the various models. To explore this possibility, we have labeled results from models that include the continuum separately from those that do not. Although the sample size is clearly much too small to draw definite conclusions, the figure weakly suggests that models with the continuum give a relatively strong $\Delta(LW_{clr,sfc})$ for a given $\Delta(PW)$. Figure 7 shows how $\Delta(LW_{sfc})$ correlates with $\Delta(PW)$. Here the sample size is somewhat larger, since more models reported $\Delta(LW_{sfc})$ than $\Delta(LW_{clr,sfc})$. Again in Figure 7, results from models that include the continuum are labeled separately from those that do not. We are unable to draw any strong conclusions from this figure. Presumably, strong geographical variations are at work here, so that global means tell little. There are two conspicuous "outliers," namely, the BMRC model [with a very small $\Delta(PW)$] and NCAR's CCM0 (with a very large $\Delta(PW)$). If we omit these two models from the sample, there is a very clear tendency for $\Delta(LW_{sfc})$ to increase as $\Delta(PW)$ increases.

Taken together, these results suggest that for each model, $\Delta(LW_{sfc})$ is mainly determined by $\Delta(PW)$, although the particular values obtained depend on the radiation parameterization used.

After the largest and smallest values for each flux have been discarded, the means are as follows:

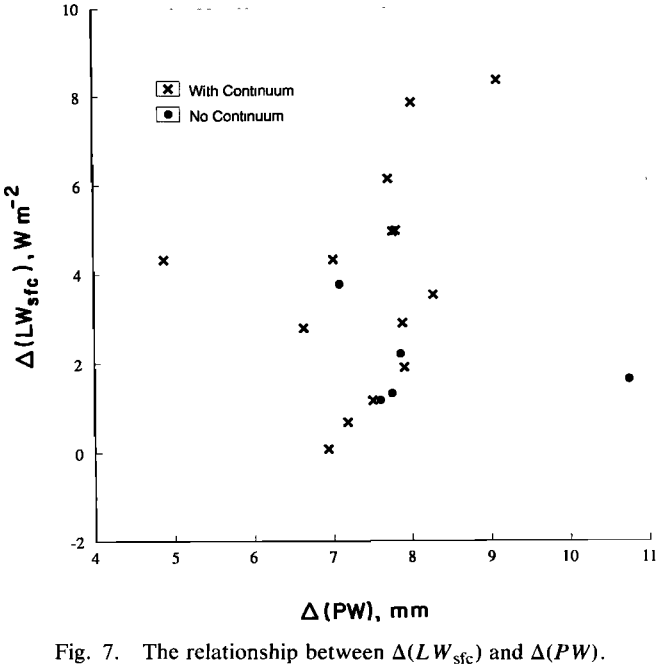

Fig. 7. The relationship between $\Delta(LW_{sfc})$ and $\Delta(PW)$.

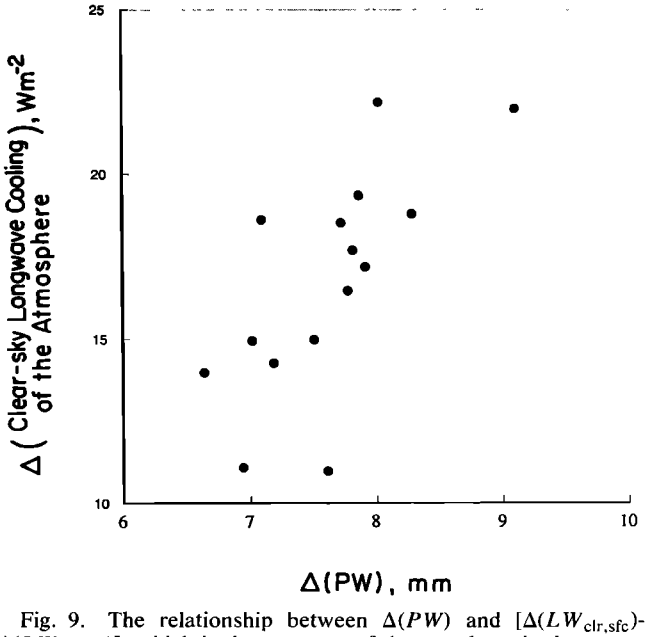

Fig. 9. The relationship between $\Delta(PW)$ and $[\Delta(LW_{clr,sfc})-\Delta(LW_{clr,top})]$, which is the response of the net clear sky longwave cooling of the atmosphere.

TABLE 5. The Globally Averaged $P(-2)$ and $PW(-2)$

+2 K RUNS	CCC	CSU 9L	CSU 17L	GFDL I	GFDL II	ECHAM Diag.	ECHAM Prog.	CCM/ LLNL	MRI	NCAR CCM0
P, mm d^{-1}	2.59	3.57	3.69	2.36	2.80	2.25	2.12	3.24	2.95	3.40
PW, mm	24.17	21.17	20.93	19.53	17.10	20.65	21.53	19.65	23.55	26.35

Precipitation units are millimeters per day and precipitable water units are millimeters.

$$\Delta(N) = -7.61 \text{ W m}^{-2}$$

$$\Delta(SW) = 0.39 \text{ W m}^{-2}$$

$$\Delta(LW) = 3.29 \text{ W m}^{-2}$$

$$\Delta(SH) = 1.77 \text{ W m}^{-2}$$

$$\Delta(LH) = -12.15 \text{ W m}^{-2}.$$

This list makes it clear that the sign and magnitude of $\Delta(N)$ are driven primarily by $\Delta(LH)$. Figure 8 shows the relationship between $\Delta(N)$ and $\Delta(LH)$. There is relatively little order; if it is true that for each model, $\Delta(N)$ is driven by $\Delta(LH)$, the details of the coupling differ from model to model sufficiently to account for the considerable scatter in Figure 8. Of course, the standard deviations of the various radiative responses are also large.

The second most important contribution to $\Delta(N)$ comes from $\Delta(LW)$ which, as we have seen, is closely related to $\Delta(PW)$. Thus we conclude that the two most important contributions to $\Delta(N)$ are closely tied to the hydrologic cycle.

This conclusion merely reaffirms the well-known facts that to a first approximation the speed of the evaporation-precipitation cycle is determined by the rate at which latent heating is required to balance the radiative cooling of the atmosphere and that the latter is strongly influenced by the moisture content of the atmosphere. Figure 9 demonstrates that increasing PW favors stronger radiative cooling of the atmosphere.

As an example, compare the MRI model with the two versions of the CSU model. This comparison is interesting because the two models use essentially the same convective parameterization, but the MRI model does not include the effects of the continuum, while the CSU model does. The MRI model produces about 15% less $P(-2)$ than the CSU models (Table 5).

Harshvardhan et al. [1989] reported the results of an experiment with the CSU model in which the effects of the continuum were artificially suppressed. The strong change in the surface longwave radiation, corresponding to reduced cooling of the atmosphere in the experiment, was balanced primarily by a reduction in the surface latent heat flux. This mutual adjustment between longwave radiation and the surface latent heat flux should be interpreted in terms of the atmospheric energy budget, rather than the surface energy budget, because the SSTs were fixed in the experiment.

Again, these results were largely anticipated by *Ramanathan* [1981], who identified the tendency for a synergistic compensation between increased radiative cooling of a moister atmosphere and an increased surface latent heat flux.

5. Zonally Averaged Responses

The overwhelming importance of the hydrologic cycle for the various surface energy budget results discussed above motivates us to investigate the simulations of P and PW in more detail. Figures 10 and 11 show the zonally averaged distributions of $P(-2)$ and $PW(-2)$, as obtained with the various models; and Figures 12 and 13 give the corresponding values of $\Delta(P)$ and $\Delta(PW)$.

Despite certain gross similarities the differences among the models are very large. For the -2 K runs the maximum zonally averaged precipitation rates in the tropical rainbands range from about 3.5 mm d^{-1} in the Hamburg model to about 10 mm d^{-1} in the LMD model. The range of the zonally averaged values of $P(-2)$ in the mid-latitude storm belts is similarly spectacular, especially for the northern (summer) hemisphere, where convective precipitation is significant. The tropical maximum of the zonally averaged $PW(-2)$ ranges from about 28 mm in the Hamburg model to 48 mm in the LMD model. Despite the previously noted lack of high correlation between the global means of $P(-2)$ and $PW(-2)$, the highest and lowest tropical values of $P(-2)$ occur in the same pair of models that have the highest and lowest tropical values of $PW(-2)$.

When the SST is increased from -2 K to $+2$ K, the response of the zonally averaged precipitation rate, in all of the models, is an increase at nearly all latitudes. The magnitude of the tropical response varies enormously among the models, however. The response of PW is again an increase at all latitudes. Roughly speaking, the tropical PW responds to a 4 K increase in SST by increasing by about 50%. Although the tropical values of $\Delta(PW)$ range over about 30% among the various models, there is, overall, somewhat better agreement on $\Delta(PW)$ than on $\Delta(P)$. The drastic increase of the tropical PW is arguably the strongest and most nearly unanimous response exhibited by the models. It can be qualitatively explained by the dependence of

TABLE 6. The Globally Averaged $\Delta(P)$ and $\Delta(PW)$

+2 K MINUS −2 K	CCC	CSU 9L	CSU 17L	GFDL I	GFDL II	ECHAM Diag.	ECHAM Prog.	CCM/ LLNL	MRI	NCAR CCM0
P, mm d^{-1}	0.33	0.69	0.68	0.42	0.42	0.31	0.29	0.43	0.38	0.29
PW, mm	8.29	9.11	8.03	7.02	6.64	7.19	7.51	7.10	7.76	10.75

Precipitation units are millimeters per day and precipitable water units are millimeters.

As Simulated by the Various Model

UKMO	DMN/ CNRM	OSU/ IAP	BMRC	LMD	ECMWF	GISS	DNM	MGO	Mean	SD
3.08	2.79	2.55	3.29	2.81	2.08	2.86	2.18	2.66	2.79	0.43
20.54	20.92	27.09	20.71	25.15	21.76	21.80	21.68	22.14	21.90	1.88

the saturation vapor pressure on SST, together with an assumed constant relative humidity [e.g., *Stephens and Greenwald*, 1991].

Figures 14 and 15 show the zonally averaged distributions of $LW_{clr,sfc}(-2)$ and $\Delta(LW_{clr,sfc})$, respectively. Except for the CCC model (in high latitudes) and the LMD model (in the tropics) the various GCMs agree reasonably well on $(LW_{clr,sfc})(-2)$. They disagree significantly, however, on $\Delta(LW_{clr,sfc})$, although all models do agree that $\Delta(LW_{clr,sfc}) > 0$ (the clear sky LW cooling of the surface decreases) at virtually all latitudes. The two CSU models produce a tropical $\Delta(LW_{clr,sfc})$ of about 20 W m^{-2}, significantly more than any of the other models. This strong positive $\Delta(LW_{clr,sfc})$ may be a consequence of the models' unique boundary layer parameterization, in which the humid air near the surface is incorporated into a variable depth mixed layer, and their lack of vertical moisture diffusion above the planetary boundary layer (PBL). These elements of the model's formulation act to confine any increased moisture content to a relatively thin layer near the surface, where it can readily influence $LW_{clr,sfc}$.

6. Influence of the Convection Parameterization

Our results show that the simulated response of the surface energy budget to a 4 K warming of the ocean varies widely depending on the response (and therefore depending on the parameterized formulation) of the model's hydrologic cycle.

A key element of any model's hydrologic cycle is its parameterization of cumulus convection. The role of cumulus convection in the atmospheric general circulation can be viewed in several complementary ways. It transports energy from near the surface to the troposphere [e.g., *Riehl and Malkus*, 1958]. It contributes a large fraction of the global precipitation. It constrains the thermodynamic structure of the atmosphere, preventing the lapse rate of temperature from becoming "too" strong and limiting the atmospheric humidity [*Arakawa and Chen*, 1987]. It transports moisture upward from the PBL into the free atmosphere and deposits vapor, liquid, and ice aloft [e.g., *Arakawa and Schubert*, 1974], thus strongly influencing the distribution of stratiform clouds. In short, cumulus convection is by far the single most powerful agency of the hydrologic cycle.

With this in mind we have investigated the role of convective parameterizations in determining the results discussed in the previous sections. We have divided the models used in this study into three camps (see Table 1): those that use convection schemes based on the "mass flux" approach [*Arakawa*, 1969], those that use some version of the "Kuo parameterization" [*Kuo*, 1965], and those that use moist convective adjustment [*Manabe et al.*, 1965]. Versions of the mass flux approach have been adopted in 8 of the 19 models discussed in this study: OSU/IAP, the two CSU models, GISS, MRI, UKMO, ECMWF, and DMN/CNRM. Versions of the Kuo parameterization are used by five of the models: ECHAM PROG, ECHAM DIAG, BMRC, LMD, and MGO. The remaining six models use moist convective adjustment.

Figure 16 shows how $\Delta(PW)$ varies with $\Delta(P)$ and indicates which convection parameterization is used by each model (see figure legend). The mass flux schemes agree fairly well on $\Delta(PW)$, a value near 8 mm is preferred, and only the 9-level version of the CSU model gives a slightly different value. The models with mass flux parameterizations seem to select this particular $\Delta(PW)$ but do not strongly couple $\Delta(P)$ with $\Delta(PW)$.

With both the Kuo parameterization and the moist convective adjustment, $\Delta(PW)$ takes a range of values and tends to decrease as $\Delta(P)$ increases. This suggests that with these two parameterizations the increase of the precipitation rate tends to limit the increase of the precipitable water. In the case of the Kuo scheme, the mutual variations of $\Delta(P)$ and $\Delta(PW)$ may arise from different formulations of the moisture storage parameter. In the case of moist convective adjustment the mutual variations may arise from different critical relative humidities imposed as criteria to trigger the adjustment. Obviously, these interpretations are extremely tentative; they do suggest avenues for further research, however.

7. Summary and Conclusions

For 19 GCMs we have identified major differences in the responses of the various components of the surface energy flux to a 4 K warming of the sea surface temperature. These differences among the models have been traced, to a large degree, to differences in their simulated hydrologic cycles and in their parameterizations of longwave radiation (especially the water vapor continuum) and cumulus convection. These conclusions are consistent with those of *Gutowski et al.* [1991].

Our analysis of $\Delta(N)$, the response of the net surface energy flux to an SST increase, indicates that cloud-radiation effects are of secondary importance. This is in strong con-

As Simulated by the Various Models

UKMO	DMN/ CNRM	OSU/ IAP	BMRC	LMD	EC/LLNL	GISS	DNM	MGO	Mean	SD
0.55	0.55	0.39	0.48	0.37	0.40	0.41	0.31	0.34	0.42	0.10
7.73	7.78	7.87	4.88	7.92	7.82	7.90	7.61	6.94	7.66	0.58

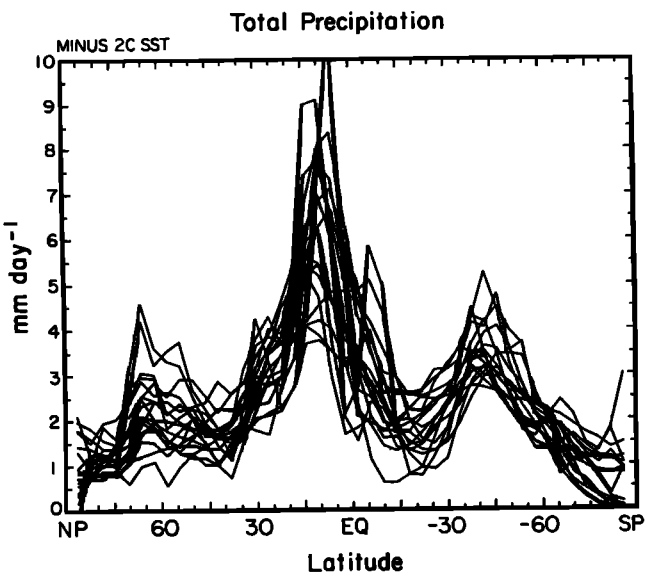

Fig. 10. The zonally averaged distribution of $P(-2)$. Each line represents one model result. The main purpose of this figure is to show the range of variation among the various models.

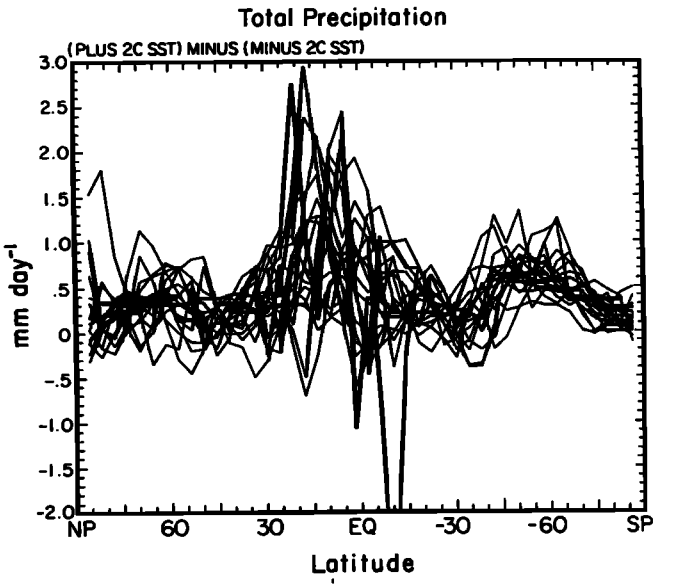

Fig. 12. As in Figure 10 but for the zonally averaged distribution of $\Delta(P)$.

trast to the conclusions of C90, who showed that the net radiative response at the top of the atmosphere, denoted by G, varied among the models mainly as a result of cloud effects. There is no contradiction between our results and those of C90. In fact, it is worth noting that the uncertainties of G and $\Delta(N)$, as indicated by disagreements among the GCMs, are both associated with moist processes: the former with the cloud radiative forcing and the latter with the speed of the hydrologic cycle.

We conclude therefore that major differences in the climate sensitivities of existing atmospheric GCMs are, to a large extent, directly due to differences in their parameterizations of moist processes and closely related radiative processes. These formulation differences arise from disagreements, within the scientific community, concerning the most realistic way to formulate the relevant moist physics. Such disagreements are a natural and even healthy component of the scientific enterprise. They arise from and, in effect, serve to identify deficiencies in our collective physical understanding.

The wide range of model sensitivities uncovered in the present study and that of C90 cannot be narrowed simply by increasing model resolution; improvements in the model physics will be required to improve the simulated climate. Our results strongly suggest that if at some future time all of the participating models could be run with drastically increased resolution, the differences in their climate sensitivities would be quite comparable to those discussed here. We note the recent study by *Tibaldi et al.* [1990], who found that although the deterministic forecast skill of the ECMWF model progressively improves as the resolution is increased

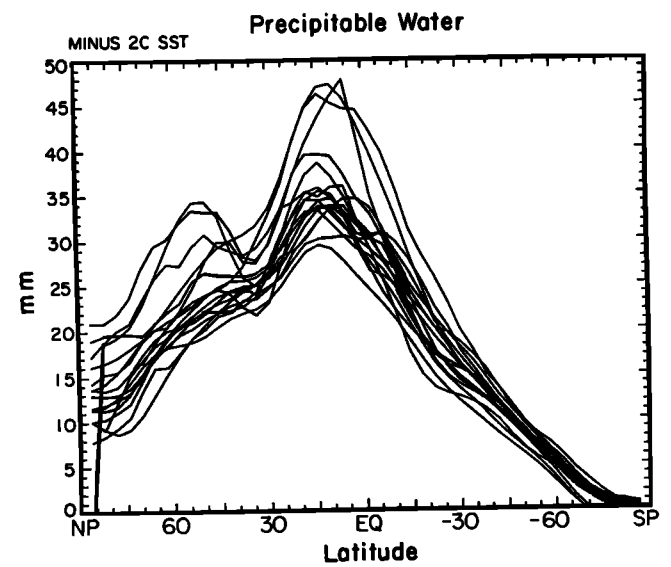

Fig. 11. As in Figure 10 but for the zonally averaged distribution of $PW(-2)$.

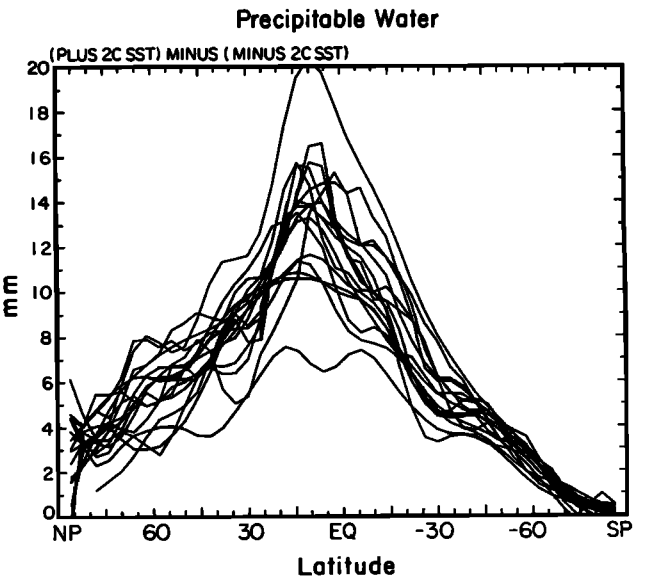

Fig. 13. As in Figure 10 but for the zonally averaged distribution of $\Delta(PW)$.

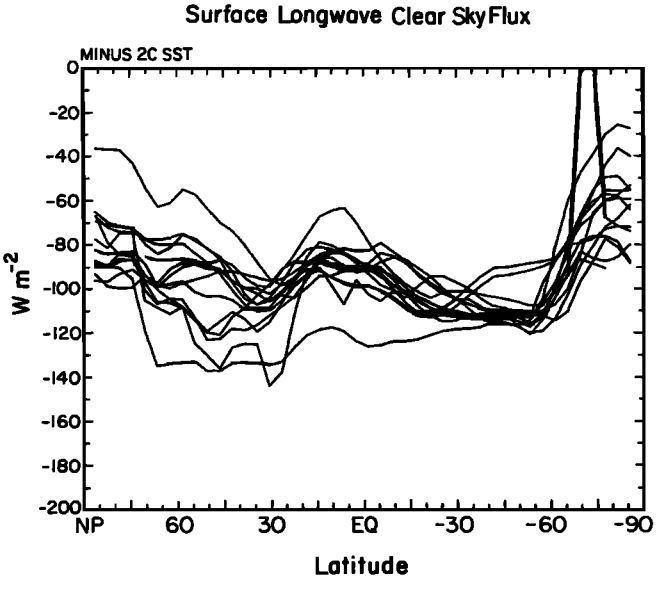

Fig. 14. As in Figure 10 but for the zonally averaged distribution of $LW_{clr,sfc}(-2)$.

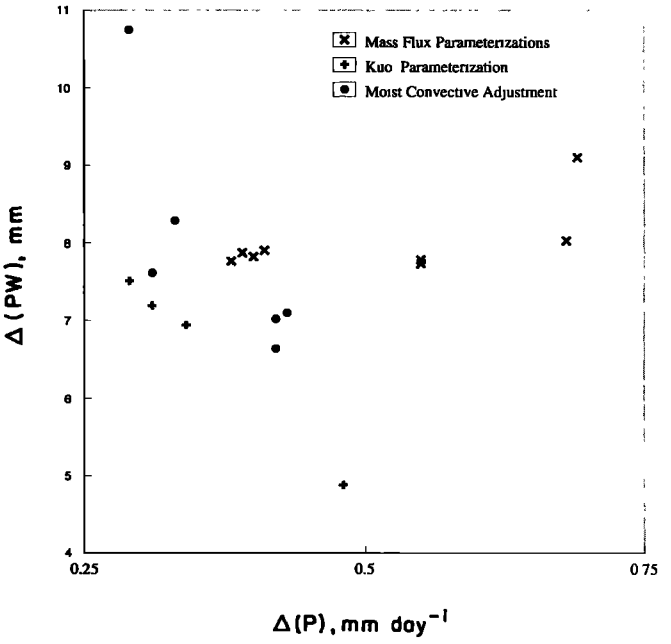

Fig. 16. Scatter diagram showing $\Delta(P)$ and $\Delta(PW)$ for the various models.

from T21 to T106, the systematic error of the model, which represents the deficiencies of the simulated climate, improves as the resolution is increased from T21 to T63 (also see *Boville* [1991]) but does not improve much further as the resolution is increased from T63 to T106. This implies that dramatically increased computer power would not, by itself, be sufficient to greatly improve either our ability to simulate the present climate or our confidence in climate change simulations produced by existing models. Improvements in climate simulation and climate forecasting must come primarily from improved understanding of the physics of the climate system.

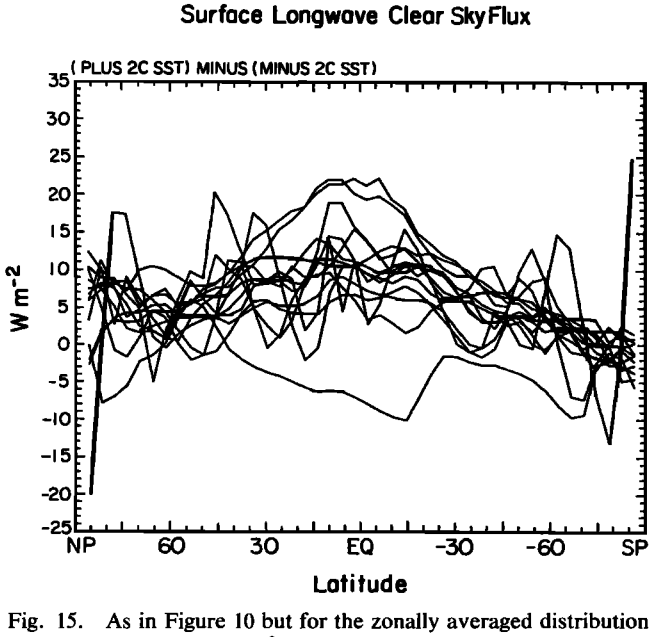

Fig. 15. As in Figure 10 but for the zonally averaged distribution of $\Delta(LW_{clr,sfc})$.

Acknowledgments. This GCM intercomparison project was initiated under the auspices of the Atmospheric and Climate Research Division, U. S. Department of Energy, under grant DE-FG02-89-ER69027 to Colorado State University, grant DE-FG0285-ER60314 to SUNY Stony Brook, interagency agreement DE-AI05-90ER61068 to the Goddard Institute for Space Studies, contract W-7405-ENG-48 to Lawrence Livermore National Laboratory, and contract DE-AI01-80EV10220 to the National Center for Atmospheric Research, which is sponsored by the National Science Foundation. Further support was provided by NASA's Climate Program under grant NAG 1-1266 to Colorado State University, by the Bundesminister für Forschung und Technologie, Germany, through grant KF20128 to the University of Hamburg, and by the Commission of European Communities through contract EV4C-066-F to DMN/CNRM. Computing resources were also provided to Colorado State University by the Numerical Aerodynamic Simulation Program at NASA Ames Research Center.

REFERENCES

Arakawa, A., Parameterization of cumulus convection, *Proc. WMO/IUGG Symp. Numer. Weather Predict.*, *4*(8), 1–6, 1969.

Arakawa, A., and J.-M. Chen, Closure assumptions in the cumulus parameterization problem, in Short and Medium Range Numerical Weather Prediction, *J. Meteorol. Soc. Jpn.*, spec. vol., 1987.

Arakawa, A., and W. H. Schubert, The interaction of a cumulus cloud ensemble with the large-scale environment, I, *J. Atmos. Sci.*, *31*, 674–701, 1974.

Boville, B., Sensitivity of simulated climate to model resolution, *J. Climate*, *4*, 469–485, 1991.

Cess, R. D., and G. L. Potter, Exploratory studies of cloud radiative forcing with a general circulation model, *Tellus*, *39*(A), 460–473, 1987.

Cess, R. D., et al., Interpretation of cloud-climate feedback as produced by 14 atmospheric general circulation models, *Science*, *245*, 513–516, 1989.

Cess, R. D., et al., Intercomparison and interpretation of climate feedback processes in 19 atmospheric general circulation models, *J. Geophys. Res.*, *95*, 16,601–16,615, 1990.

Ellingson, R. G., J. Ellis, and S. Fels, The intercomparison of radiation codes in climate models (ICRCCM): Longwave results, *J. Geophys. Res.*, *96*, 8925–8928, 1991.

Fouquart, Y., B. Bonnel, and V. Ramaswamy, Intercomparing

shortwave radiation codes for climate studies, *J. Geophys. Res.*, *96*, 8955–8968, 1991.

Gutowski, W. J., D. S. Gutzler, D. Portman, and W. C. Wang, Surface energy balances of three general circulation models: Implications for simulating regional climate change, *J. Clim.*, *4*, 121–134, 1991.

Hansen, J., G. Russell, D. Rind, P. Stone, A. Lacis, S. Lebedeff, R. Ruedy, and L. Travis, Efficient three-dimensional global models for climate studies: Models I and II, *Mon. Weather Rev.*, *111*, 609–662, 1983.

Harshvardhan, D. A. Randall, T. G. Corsetti, and D. A. Dazlich, Earth radiation budget and cloudiness simulations with a general circulation model, *J. Atmos. Sci.*, *46*, 1922–1942, 1989.

Houghton, J. T., G. J. Jenkins, and J. J. Ephraums (Eds.), *Climate Change: The IPCC Scientific Assessment*, 365 pp., Cambridge University Press, New York, 1990.

Kuo, H. L., On formation and intensification of tropical cyclones through latent heat release by cumulus convection, *J. Atmos. Sci.*, *22*, 40–63, 1965.

Manabe, S., J. Smagorinsky, and R. F. Strickler, Simulated climatology of a general circulation model with a hydrologic cycle, *Mon. Weather Rev.*, *93*, 769–798, 1965.

Mitchell, J. F. B., and W. I. Ingram, On CO_2 and climate change: Mechanisms of changes in cloud, *J. Clim.*, in press, 1991.

Mitchell, J. F. B., C. A. Wilson, and W. M. Cunnington, On CO_2 climate sensitivity and model dependence of results, *Q. J. R. Meteorol. Soc.*, *113*, 293–322, 1987.

Ramanathan, V., The role of ocean-atmosphere interactions in the CO_2 climate problem, *J. Atmos. Sci.*, *38*, 918–930, 1981.

Ramanathan, V., and W. Collins, Thermodynamic regulation of ocean warming by cirrus clouds deduced from observations of the 1987 El Nino, *Nature*, *351*, 27–32, 1991.

Ramanathan, V., R. D. Cess, E. F. Harrison, P. Minnis, B. R. Barkstrom, E. Ahmad, and D. Hartmann, Cloud-radiative forcing and climate: Results from the Earth Radiation Budget Experiment, *Science*, *243*, 57–63, 1989.

Riehl, H., and J. S. Malkus, On the heat balance in the equatorial trough zone, *Geophysica*, *6*, 503–537, 1958.

Stephens, G. L., and T. J. Greenwald, The Earth's radiation budget and its relation to atmospheric hydrology, 1, Observations of the clear sky greenhouse effect, *J. Geophys. Res.*, *96*(D8), 15,311–15,340, 1991.

Tibaldi, S., T. N. Palmer, C. Brankovic, and U. Cubasch, Extended-range prediction with ECMWF models: Influence of horizontal resolution on systematic error and forecast skill, *Q. J. R. Meteorol. Soc.*, *116*, 835–866, 1990.

J. P. Blanchet and G. J. Boer, Canadian Climate Center, Atmospheric Environment Service, Department of the Environment, 4905 Dufferin Street, Downsview, Ontario M3H 5T4, Canada.

R. D. Cess and M.-H. Zhang, Institute for Terrestrial and Planetary Atmospheres, State University of New York, Stony Brook, NY 11794-2300.

D. A. Dazlich and D. A. Randall, Department of Atmospheric Science, Colorado State University, Fort Collins, CO 80523.

A. D. DelGenio and A. A. Lacis, Goddard Institute for Space Studies, National Aeronautics and Space Administration, 2880 Broadway, New York, NY 10025.

M. Deque and J. F. Royer, Direction de la Meteorologie, Centre National de Recherches Meteorologiques, 42 Av. Coriolis, 31057 Toulouse Cedex, France.

V. Dymnikov and V. Galin, Department of Numerical Mathematics, Academy of Sciences, 29 Ryleeva Street, Moscow 119034, Russia.

S. J. Ghan, G. L. Potter, and K. E. Taylor, Program for Climate Model Diagnosis and Intercomparison, Lawrence Livermore National Laboratory, P. O. Box 808, L-264, Livermore, CA 94550.

H. Le Treut and Z.-X. Li, Laboratoire de Meteorologie Dynamique, 24 Rue Lhomond, 75231 Paris Cedex, France.

X.-Z. Liang, Department of Mechanical Engineering, State University of New York, Stony Brook, NY 11794-2300.

B. J. McAvaney and L. Rikus, Bureau of Meteorology Research Centre, GPO Box 1289K, Melbourne, Victoria 3001, Australia.

V. P. Meleshko, D. A. Sheinin, and A. P. Sokolov, Voeikov Main Geophysical Observatory, 7 Karbisheva, St. Petersburg 194018, Russia.

J. F. B. Mitchell, Meteorological Office, Met O 20, London Road, Bracknell, Berkshire RG12 2SZ, England.

J.-J. Morcrette, European Centre Medium-Range Weather Forecasts, Reading, Berkshire RG2 9AX, England.

E. Roeckner and U. Schlese, Meteorologisches Institut, University of Hamburg, Bundesstrasse 55, D 2000, Hamburg 13, Germany.

J. Slingo, Department of Meteorology, University of Reading, Reading, Berkshire RG6 2AU, England.

W. M. Washington, Climate and Global Dynamics Division, National Center for Atmospheric Research, P. O. Box 3000, Boulder, CO 80307-3000.

R. T. Wetherald, National Oceanic and Atmospheric Administration/Geophysical Fluid Dynamics Laboratory, Princeton University, P. O. Box 308, Princeton, NJ 08540.

I. Yagai, Meteorological Research Institute, 1-1 Nagamine, Tsukuba, Ibakari-Ken 305, Japan.

(Received July 18, 1991;
revised November 27, 1991;
accepted December 2, 1991.)